

## Article

# Verification of the Inverse Scale Effect Hypothesis on Viscosity and Diffusion by Azo-Amino Acid Schiff Base Copper Complexes

Yoshitora Wadayama, Ai Kaneda, Taiga Imae, Daisuke Nakane and Takashiro Akitsu \* 

Department of Chemistry, Faculty of Science, Tokyo University of Science, 1-3 Kagurazaka, Shinjuku-ku, Tokyo 162-8601, Japan

\* Correspondence: akitsu2@rs.tus.ac.jp

**Abstract:** Microdroplets generated in microfluidic devices are attracting attention as a new chemical reaction field and are expected to improve reactivity. One of the effects of microscaling is that the ratio of the force that acts on the diffusion and movement of substances to gravity is different from that of ordinary solvents. Recently, we proposed a hypothesis for determining reaction acceleration through micro-miniaturization: If a reaction is inhibited by setting the volume and viscosity of the solution to conditions that are unfavorable to the reaction on a normal scale, that reaction can be promoted in microfluidics. Therefore, for the purpose of this verification, (1) we used an amino acid Schiff base copper(II) complex with an azobenzene group to demonstrate the polarization-induced orientation in a polymer film (the redirection that is mechanically maintained in a soft matter matrix). Numerical data on optical anisotropy parameters were reported. (2) When the reaction is confirmed to be promoted in laminar flow in a microfluidic device and its azo derivative, a copper(II) complex is used to increase the solvent viscosity or diffusion during synthesis on a normally large scale. We will obtain and discuss data on the investigation of changing the solvent volume as a region. The range of experimental conditions for volume and viscosity did not lead to an improvement in synthetic yield, nor did (3) the comparison of solvents and viscosity for single-crystal growth of amino acid Schiff base copper(II) complexes having azobenzene groups. A solvent whose viscosity was measured was used, but microcrystals were obtained using the diffusion method.



**Citation:** Wadayama, Y.; Kaneda, A.; Imae, T.; Nakane, D.; Akitsu, T. Verification of the Inverse Scale Effect Hypothesis on Viscosity and Diffusion by Azo-Amino Acid Schiff Base Copper Complexes. *J. Compos. Sci.* **2024**, *8*, 177. <https://doi.org/10.3390/jcs8050177>

Academic Editor: Francesco Tornabene

Received: 28 March 2024

Revised: 25 April 2024

Accepted: 9 May 2024

Published: 10 May 2024



**Copyright:** © 2024 by the authors. Licensee MDPI, Basel, Switzerland. This article is an open access article distributed under the terms and conditions of the Creative Commons Attribution (CC BY) license (<https://creativecommons.org/licenses/by/4.0/>).

**Keywords:** viscosity; diffusion; solvent; Schiff base complex; azobenzene

## 1. Introduction

Synthesis in microfluidic devices, which has the potential to provide certain high-throughput solutions, is attracting attention in the fields of chemistry, biology, medicine, and engineering [1–8]. Using this device, the reaction behavior is completely different from beaker-scale experimental synthesis. For example, we will look at the synthesis of glutamine Schiff base copper(II) complexes, which have already been successfully synthesized in microfluidic devices and in beaker-scale experiments. On a typical beaker scale, it is synthesized under reaction conditions of 313 K for 4 h. In contrast, microfluidic devices allow instant synthesis at room temperature [9,10].

Here, we introduce some examples of parameters from previous research. Essentially, the system is a microdroplet encapsulated within an immiscible carrier fluid [11]. In addition to requiring only a small amount of sample solution for reaction or analysis, this method has the advantage of reducing the range of solution diffusion. Droplets can essentially be viewed as isolated reaction vessels, allowing exquisite control of heat and mass transport and consideration of parameters such as temperature and time [12]. Droplet solution mixing has also been utilized in protein crystallization, heterogeneous reactions, and organic synthesis studies [13]. The success or failure of these depends on interphase mass transfer in internal convective circulation due to shear forces. Furthermore, in precision pharmaceutical synthesis applications [14], in addition to passive mixing (based

on concentration gradients), external stimuli such as voltage, magnetism, and sound may be actively applied. When active, the additional energy input promotes interfacial instability [15]. There are numerous techniques for droplet actuation, including pneumatics, thermocapillary effects, electrochemical gradients, structured surfaces, photochemical effects, dielectrophoresis, and other electrostatic techniques. These are based on surface tension adjustment, where the methodology is a favorable scaling of surface forces (in balance with gravity) [16]. It also has a high surface area to volume ratio, which shortens the transfer time and diffusion distance of heat and matter, which shortens the reaction time [17]. Non-droplet microfluidic systems, on the other hand, are characterized by inherently “laminar” and low Reynolds number flow, unlike droplets. A geometric theoretical model dealing with droplet size dependence was proposed [18]. Additionally, droplet detection and sorting are externally observable physical parameters based on impedance, fluorescence, and scattering/absorbance [19]. The droplet (formation) mechanism and also the internal reaction environment are complex and controlled by numerous conditional parameters such as surface tension, viscosity of two immiscible liquids, surface wetting properties, inertia, elasticity, and surfactant addition. However, in recent years, machine learning (ML) and artificial intelligence (AI) have begun to be used for parameter optimization as a data-driven study [20].

However, as far as we know, the method of predicting and discussing the factors of synthesis reactions promoted by microdroplets by comparing them with normal-scale reactions remains immature. This is thought to be due to the fact that at the microscale, the ratio of the force acting on the diffusion and movement of substances to gravity is different from that at the beaker scale, and the effects of heat transfer, viscous force, and surface effects are extremely large. In addition, the size of the droplet is considered to be an important parameter because it is thought to have an effect on changes in convection during synthesis. Therefore, investigating the factors that increase the reactivity of microfluidic devices is an important topic for future research, as it may be possible to perform synthesis at an alternative scale when beaker-scale synthesis is difficult due to these factors. Although this information is thought to be useful, there are few concrete examples of verification.

Therefore, in order to investigate these factors, the authors found that “If parameters set to disadvantage the reaction at the beaker scale actually have a negative effect on the reaction progress, then the parameters may be changed to favor synthesis at the microscale”. We proposed the hypothesis that “this is a contributing factor”. In order to test this hypothesis, in this study, we reexamined the polarization-induced molecular orientation in polymer films and then investigated the synthesis reaction of amino acid Schiff base copper(II) complexes on a beaker scale by adjusting the volume and viscosity of the solvent so that the reaction was unfavorable. We then decided to examine the conditions for growing single crystals of related complexes, where the azo group makes the solubility and crystal growth disadvantageous [21].

To specifically explain the aim of the “inverse scale effect hypothesis” in terms of a synthetic reaction, the volume of the solvent is set at 10 mL to 500 mL, and it is thought that the larger the solvent accumulation, the lower the reagent concentration, making the reaction disadvantageous. Regarding viscosity, it is thought that increasing the viscosity makes it difficult for convection to occur, making the reaction disadvantageous. If these reactions are adversely affected and their progress is inhibited, then reactions that must go through unfavorable solvent volume and viscosity conditions may be worth running in microfluidic devices.

In this context, this “basic” research here using soft matter or viscous matrix (solvents) aims to verify whether the proposed hypothesis is correct and is intended to be useful for the future development of microfluidic devices.

## 2. Materials and Methods

### 2.1. General Procedures

Chemicals of the highest commercial grade available (solvents from Kanto Chemical, Tokyo, Japan, organic compounds from Tokyo Chemical Industry, Tokyo, Japan, and metal sources from Wako-Fujifilm, Osaka, Japan) were used as received without further purification. Azobenzene salicylaldehyde was prepared according to methods detailed in the literature [22].

### 2.2. Preparation Complexes and Polymer Films of azo-arg (or lyz) Complexes

To a 200 mL methanol solution of azobenzene salicylaldehyde (0.2261 g, 1.00 mmol), an aqueous solution of *L*-arginine (0.1742 g, 1 mmol) or *L*-lysine (0.1462 g, 1 mmol) was added and refluxed at 373 K for a day. Then, an aqueous solution of copper(II) acetate hydrate (0.1997 g, 1.00 mmol) was added dropwise and refluxed at 373 K for a day. The resulting solution was evaporated to isolate green precipitates.

*Azo-arg* complex: Anal. found: C, 49.36; H, 4.83; N, 14.90%. Calcd for  $C_{23}H_{27}N_6CuO_7$ : C, 48.98; H, 5.00; N, 14.90%. IR (KBr):  $1625\text{ cm}^{-1}$  (N=N).

*Azo-lyz* complex: Anal. found: C, 53.14; H, 4.73; N, 11.65%. Calcd for  $C_{21}H_{24}N_4CuO_5$ : C, 52.99; H, 4.85; N, 13.47%. IR (KBr):  $1625\text{ cm}^{-1}$  (N=N).

To prepare polymer films,  $5 \times 10^{-3}$  mmol acetone solutions of these complexes (confirmed within 0.4% error of elemental analysis) and an acetone solution of Polymethyl methacrylate (PMMA) (10% *w/w*) were mixed. Thereafter, the mixed solution was dropped onto a slide glass and heated and dried on a hot plate at 323 K for 30 min to obtain a PMMA film.

### 2.3. Reaction Conditions of (azo-)gln Complexes

In an eggplant flask, a testing amount of MeOH and so on, azobenzene salicylaldehyde (0.2262 g, 1.00 mmol) or salicylaldehyde (0.1224 g, 1.00 mmol), KOH (0.0561 g, 1 mmol), and *L*-glutamine (0.1461 g, 1.00 mmol) were added and stirred at 313 K for 2 h. Then, copper(II) acetate hydrate (0.1997 g, 1.00 mmol) (and imidazole (0.0681 g, 1.00 mmol) only for the azo-gln complex) was added dropwise and refluxed at 373 K for 2 h. Yield was evaluated based on the absorbance intensity of UV–Vis spectra.

### 2.4. Crystallization Conditions of azo-leu Complex

To a 100 mL solution of MeOH, azobenzene salicylaldehyde (0.226 g, 1.00 mmol) and *L*-leucine (0.131 g, 1.00 mmol) were added and stirred at 313 K for 3 h. Then, copper(II) acetate hydrate (0.199 g, 1.00 mmol) was added and stirred at 373 K for 2 h. The resulting dark green solution was allowed to stand at 298 K for 4 days to obtain a green powder, which served for several crystallization tests.

### 2.5. Physical Measurements

An elemental analysis was performed at the Nagoya Institute of Technology. IR spectra were measured in the range of  $4000\text{--}400\text{ cm}^{-1}$  (at 298 K) using a JASCO (Tokyo, Japan) FT-IR 4200 spectrophotometer. UV–Vis spectra were measured using a JASCO (Tokyo, Japan) V-650 spectrophotometer in the range of  $700\text{--}200\text{ nm}$  (at 298 K) (yields are based on absorbance measurements). The UV light sources used were Hayashi (Tokyo, Japan) LA-410UV and LA-251Xe, equipped with a polarizing filter.

## 3. Results and Discussion

### 3.1. Polarized Light-Induced Anisotropic Molecular Orientation in Polymer Films

To date, we have aimed to develop new functions and physical properties by arranging molecules by irradiating metal complexes with polarized light and utilizing the Weigert effect (Figure 1) [22–25]. Specifically, a thin film of a metal complex and azobenzene or an azo group-containing ligand–metal complex was prepared in PMMA, and the reorientation properties in that environment were evaluated. These results suggested that, in most cases,

the Weigert effect of azobenzene may change the orientation of molecules in azo-containing complexes. However, the details of the interaction between the complex and azobenzene in the soft matter polymer film are unknown [26], and it has been difficult to investigate the mechanical properties of the complex's molecular orientation through spectroscopic measurements. Therefore, in order to reconfirm the flexible motion and anisotropic retention of the analogous (ligand) complexes (Schemes 1 and 2) under these conditions, we confirmed the polarization-induced molecular orientation using a conventional method (Figure 2).

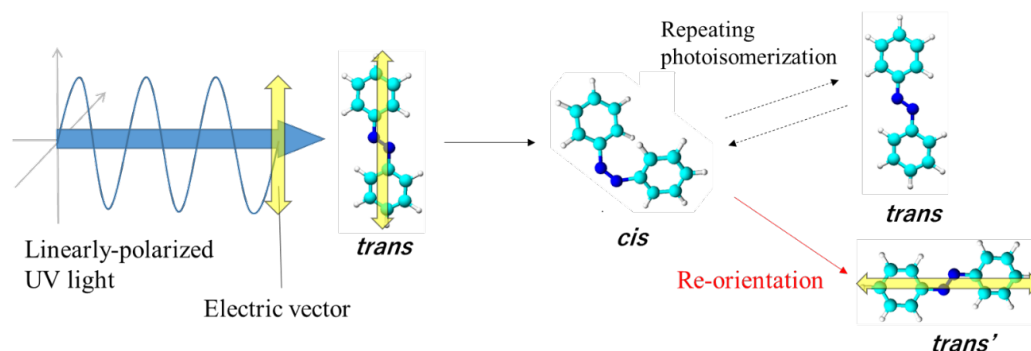
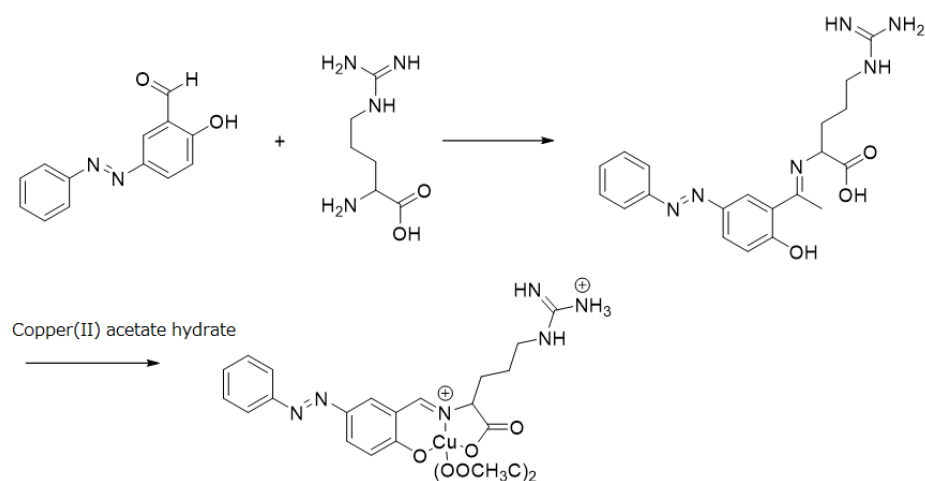
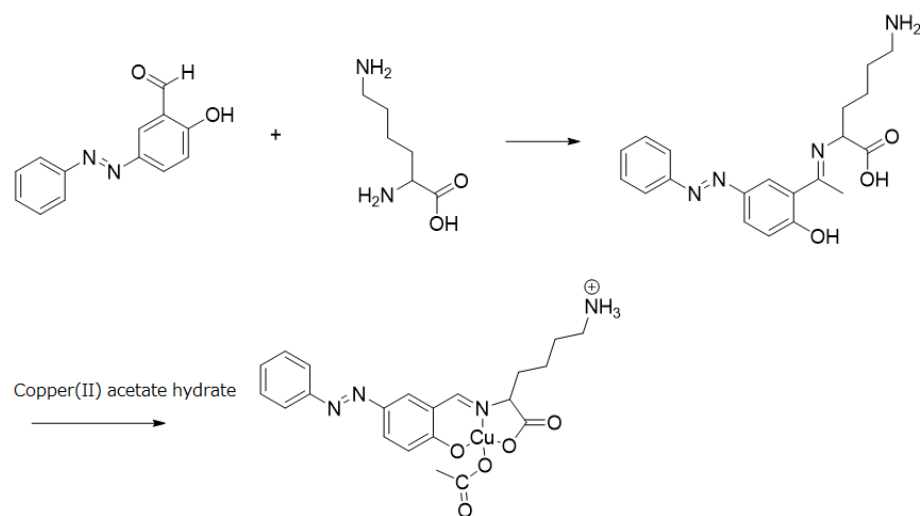


**Figure 1.** Weigert effect for azobenzene. C and N atoms were depicted as light-blue and deep-blue.



**Scheme 1.** Synthesis of azo-arg complex.



**Scheme 2.** Synthesis of azo-lyz complex.

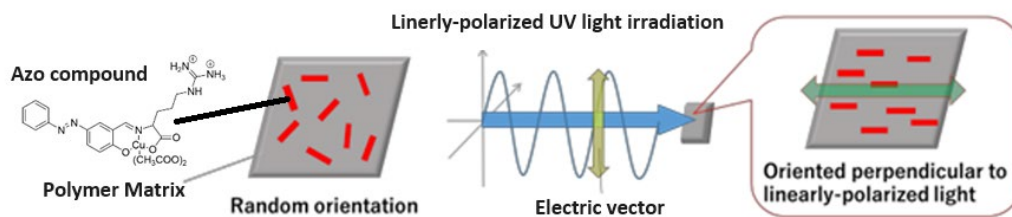


**Figure 2.** Weigert effect of an azobenzene-containing Schiff base copper(II) complex (red objects) in polymer films.

The optical state of the film was measured using a polarized UV–Vis spectrum, and the results were shown in a circular diagram to confirm the presence or absence of optical anisotropy in the film (Figures 3 and 4). The measurement results were evaluated based on the following *R* and *S* values:

$$R = A_0/A_{90}$$

$$S = (A_0 - A_{90})/(A_0 + 2 \times A_{90})$$

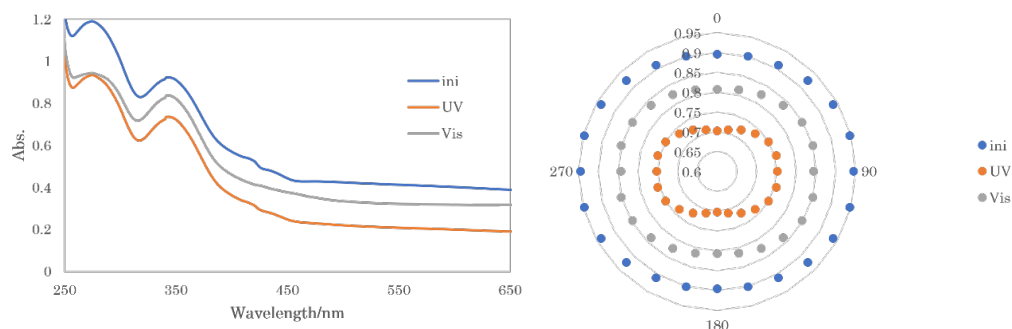


**Figure 3.** Polarized UV–Vis spectra (left) and circular plots of peak intensities (right) are shown for an azo-arg complex, measured from 0 to 90° in 15° increments. The value measured immediately after synthesis is indicated as *Ini*, the value measured after irradiation with UV light for 20 min is indicated as *UV*, and the value measured after irradiation with visible light for 20 min is indicated as *Vis*.

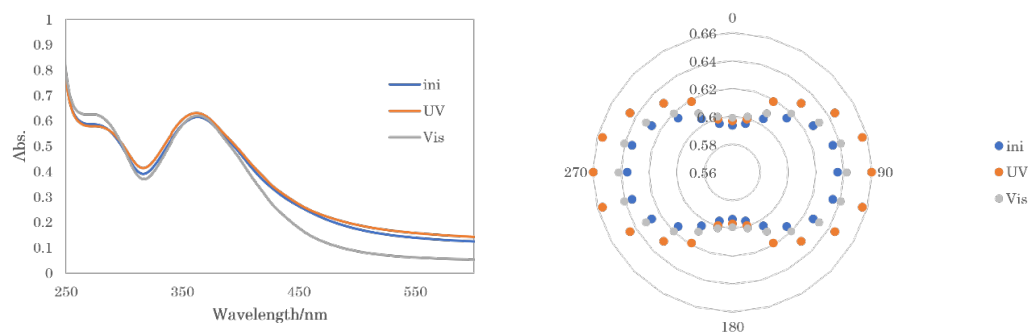


**Figure 4.** Polarized UV–Vis spectra (left) and circular plots of peak intensities (right) are shown for an azo-lyz complex, measured from 0 to 90° in 15° increments. The value measured immediately after synthesis is indicated as *Ini*, the value measured after irradiation with UV light for 20 min is indicated as *UV*, and the value measured after irradiation with visible light for 20 min is indicated as *Vis*.

Here, for both systems (Tables 1 and 2), *A*<sub>0</sub> and *A*<sub>90</sub> are the absorbances parallel to and perpendicular to the polarization plane of the irradiated light, respectively. The further the *R* parameter is from 1 and the *S* parameter is from 0, the greater the anisotropy.

**Table 1.** Anisotropic *R* and *S* parameters of arg complex.

	<b>R Parameters</b>	<b>S Parameters</b>
Ini	0.9477	−0.0177
UV	0.9326	−0.0230
Vis	0.9559	−0.0149

**Table 2.** Anisotropic *R* and *S* parameters of lyz complex.

	<b>R Parameters</b>	<b>S Parameters</b>
Ini	0.9339	−0.0225
UV	0.9043	−0.0330
Vis	0.9339	−0.0225

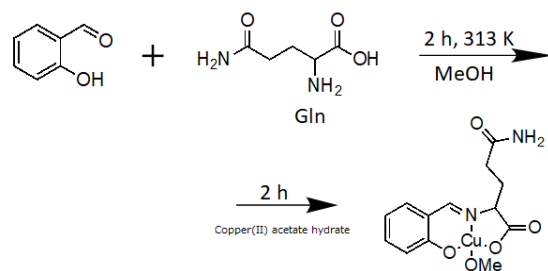
So far, we have been studying the control of molecular orientation of chiral metal complexes containing photoresponsive azobenzene by irradiation with linear/circularly polarized ultraviolet light using the Weigert effect. As is well known in liquid crystal materials, circularly polarized light with spin angular momentum can form a helical orientation with chirality [27]. In addition to chemical engineering and fluid dynamics in viscous media, there is currently insufficient chemical understanding of how to treat molecules using classical mechanics. In addition, by referring to (protein) crystal growth and molecular orientation under the conditions in droplets, it is thought that an analogy of gravity [28] and other “forces acting on objects” to molecules and nanoaggregates may be effective.

Thus, the important finding from experiments with this polymer membrane is that this system (related ligands and complexes) is suitable for discussing viscosity and diffusion on a normal scale [29]. Considering “the sum of the products of the atomic weight of each atom and the distance between the molecular center of gravity (which may be defined as the paramagnetic metal center)” may be useful. This is a quantity equivalent to the rotational moment of inertia in classical mechanics and will be newly introduced as a parameter on the molecular side in order to discuss the correlation with the quantity equivalent to the torque realized by external field orientation change.

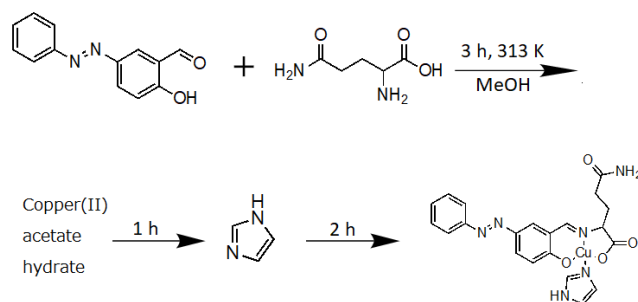
### 3.2. Synthetic Reaction Conditions

Synthetic reactions for azobenzene-containing amino acid Schiff base copper(II) complexes include an azo coupling reaction, an imine synthesis reaction, and the coordination of metal ions. Microfluidic devices do not require control of temperature or pH conditions and are known to dramatically speed up reaction rates. However, it is not always possible to synthesize it well using specific amino acids, and there is hope for microdroplets [30]. Therefore, based on negative data on amino acids that are difficult to synthesize, we must examine the possibility of accelerating the reaction by examining the presence or absence of a “reverse scale effect” based on items such as lower temperature, lower concentration, and an increased amount (namely volume) of solvents.

The reaction is set in an unfavorable direction by increasing the volume of the solvent (methanol) and decreasing the solvent concentration. The synthesis of a gln complex and an azo-gln complex (Schemes 3 and 4) was carried out in a way that disadvantaged the reaction by increasing the solvent volume and decreasing the solvent concentration. In addition, the synthesis was performed by creating a solution of ethylene glycol and methanol to increase the viscosity and make it difficult for convection to favor the reaction.



**Scheme 3.** Synthesis of a gln complex.



**Scheme 4.** Synthesis of an azo-gln complex.

From the yields of the gln complex in Table 3, the yield when synthesized with 50 mL of solvent is the highest, and the yield is about twice as high as when synthesized with other amounts of solvent. Excluding this case of 50 mL, the yield increased in the order of 10, 200, and 500 mL, which should have been in a disadvantageous direction, but the result was that the yield increased. Similarly, from the yield of the azo-gln complex in Table 4, the reaction should have progressed in an unfavorable direction by increasing the amount of solvent, but the yield increased. However, since the yield was over 100% for 200 mL and close to 100% for 500 mL, it is possible that many impurities were included.

**Table 3.** Solvent volume or viscosity dependence of yields of gln complexes.

MeOH/mL	Concentration of MeOH Solution/%	Viscosity/ mPa·s	Yield/g	Yield/%
10			0.111	30.97
50			0.2888	83.91
200			0.1282	35.73
500			0.1528	43.73
	100	0.36	0.2888	83.91
	50	2.39	0.380	>100

**Table 4.** Solvent volume or viscosity dependence of yields of azo-gln complexes.

MeOH/mL	Concentration of MeOH Solution/%	Viscosity/ mPa·s	Yield/g	Yield/%
10			0.2981	61.67
50			0.3006	62.56
200			0.5219	>100
500			0.4488	93.01
	100	0.36	0.3006	62.56
	50	2.39	0.5297	>100

A solution of ethylene glycol and methanol was made, and the reaction was set in an unfavorable direction by increasing the viscosity and making convection difficult [31]. Ethylene glycol added to the methanol solvent to increase the viscosity of the solvent has

low volatility, and it is impossible to dry the solution after synthesis to obtain the product. Therefore, using the complex synthesized in pattern 1, a calibration curve for the derivative copper(II) complex and a calibration curve for the azo-containing gln derivative copper(II) complex were created, and the yield was measured from the absorbance of the solution synthesized in pattern 2. In addition, when conducting the experiment in pattern 2, it was carried out using a solvent amount of 50 mL, which had a good yield in pattern 1, and ethylene glycol was added to create a 50% methanol solution. Looking at the results, as in pattern 1, we increased the viscosity and set the reaction in an unfavorable direction, but the yield increased. Since this result also exceeded 100% yield (>100 in the Table 3), it is thought that the solution after synthesis contained impurities.

First, we will consider the results to determine if this hypothesis is considered correct. The results showed that even if the parameters were set to disadvantage the reaction on a beaker scale, the progress of the reaction was not adversely affected. Therefore, the two parameters verified this time, volume and viscosity, are considered not to be advantageous for microscale synthesis. Next, we will consider a case in which this hypothesis is considered incorrect. In this case, it is possible that the differences in the environments between the beaker scale and the microscale are so large that things that are greatly affected at the microscale were not treated as considerations at the beaker scale.

The working hypothesis [22] is that “If a parameter set to disadvantage the reaction at the beaker scale actually has a negative effect on the progress of the reaction, then that parameter is a factor that favors synthesis at the microscale”. Our goal here is to synthesize metal complexes and protein composite materials within microdroplets using a microfluidic device and to further control these droplets using flow channels and external physical stimuli, which are common in this field. It is necessary to apply the classical mechanical parameters introduced in the experiment (degree of viscosity, distance of diffusion) and verify how miniaturization from the micro- to nanoscale is reflected in the laws of fluid mechanics.

It cannot be denied that, under even more extreme high-viscosity conditions, the difference may be clearly observed. However, microfluidic devices use normal solvents, and we employed experimental conditions based on the idea that viscosity conditions that deviate extremely from these would deviate from the purpose of hypothesis testing to examine the effects of mechanics and diffusion.

### 3.3. Crystallization Conditions

Low-molecular-weight organic compounds are overwhelmingly crystallized in solution. Various factors can be considered to produce large, high-quality crystals. Crystallization conditions are determined by a combination of these factors. In general, when few crystal nuclei are generated and they grow slowly, good-quality and large crystal nuclei can be obtained. The key point here is the degree of supersaturation of the solution [32]. The crystal growth rate also determines the quality and size of the crystal.

If small but relatively good crystals have been obtained in the past but the crystal growth does not proceed as expected, the crystals obtained in the past can be used as seed crystals to grow larger crystals. There are many. The size of the seed crystal has a large effect on subsequent crystal growth, but determining how crushed it should be depends on trial and error.

Crystallization progresses through the process from nucleation to crystal growth [33]. If nucleation does not go well, an amorphous material may be formed and crystals may not be obtained. Crystal growth progresses as the solid–liquid equilibrium approaches the solid, and this rate also depends on various forces on the crystal surface, the concentration of molecules that are precipitating, and the properties of the solvent surrounding the crystal. Crystals have surfaces that grow easily and surfaces that do not, and the surface that grows quickly is the surface on which the crystallizing molecules bond tightly. Due to this difference in growth rate, crystals that have grown to a large size will have several external shapes.

To crystallize from a solution, first prepare a near-saturated solution of the molecules you want to crystallize, and then slowly bring the solution to a supersaturated state. By doing so, a small number of good single crystals can be obtained.

When the vapor pressure of the solvent reaches equilibrium, the poor solvent diffuses into the solution in the inner container through the vapor phase, causing saturation or supersaturation and crystallization. A leucine (leu-)derivative complex (*azo-leu complex*, Figure 5) was employed, and in addition to crystallization and structural analysis using conventional vapor diffusion methods, conditions such as convection and diffusion were investigated by changing solvent viscosity to mimic gel layer crystallization [34]. First, we investigated the presence or absence of rough (almost qualitative) changes in viscosity after mixing various solutes (liquid substances that increase viscosity) with MeOH and DMF, which are typical good solvents (Table 5).

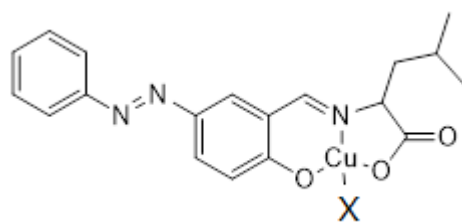


**Figure 5.** Structure of azo-leu complex (X denotes solvents using crystallization to coordinate potentially).

**Table 5.** Viscosity changes of mixed solvents after addition to MeOH or DMF.

Added Solvents	To MeOH	To DMF
Heptane	No change	Impossible to mix
1,2-Dimethoxybenzene	Little change	Impossible to mix
$\beta$ -Gluconolactone	Little change	Impossible to mix
Ethylene glycol	Changed	Changed
Polyvinyl alcohol	Little change	Little change
Polyethylene glycol 2000	Little change	Little change
Polyvinylpyrrolidone K90	No change	No change
Polyvinyl chloride	Impossible to mix	Little change
Liquid paraffin	Impossible to mix	Little change

Solvent evaporation method [35]: This is the simplest and most effective method to obtain good crystals. The rate of crystal growth is adjusted by controlling the initial solution concentration, temperature, evaporation rate, etc., and it is generally good to set the time required for crystallization from several hours to several days. Indeed, we have obtained single crystals of “similar” copper(II) complexes suitable for X-ray analysis [21].

Vapor diffusion method [36]: In this method, a solution of the molecules to be crystallized is placed in a small container and placed inside a larger, sealed container. The small inner container is left open, and the outer container is filled with a volatile antisolvent that can mix with the dissolved solvent in which the molecules are dissolved.

Initially, the solvent evaporation method was used. Crystallization was performed under three conditions in which the crystal growth rate varied depending on the initial solution concentration and evaporation rate. After trying several solutions, needle-shaped crystals were observed in methanol and THF under the slow crystal growth rate condition. We tested the hypothesis that increasing the viscosity of the solvent slows down the diffusion and aggregation of the solute, resulting in larger single crystals. On the contrary, the highly viscous solvent obtained by adding ethylene glycol to MeOH actually produces better crystals (Table 6).

**Table 6.** Conditions and results of the solvent evaporation method.

Solvent	Added Compound	Temperature/K	Viscosity/ mPa·s	Results
MeOH	None	317.3	0.82	Small
MeOH	Ethylene glycol	317.2	0.95	Not Appeared
MeOH	Ethylene glycol	317.8	1.18	Not Appeared
MeOH	Ethylene glycol	317.9	1.10	Not Appeared
MeOH	Ethylene glycol	317.3	1.52	Not Appeared

Next, the vapor diffusion method was performed. In the vapor diffusion method, crystals were crystallized under two conditions, varying the crystal growth rate depending on the size of the container. Here, needle-shaped crystals [37] were confirmed in methanol with diethyl ether vapor diffusion and in DMF with diethyl ether vapor diffusion. Crystals were obtained only in the methanol condition, with slow crystal growth. In DMF, crystals were confirmed in both conditions, but the slower crystal growth condition resulted in cleaner crystals, and, furthermore, the reproducibility was very high. However, the sizes of the crystals themselves were all quite small.

Based on these results, we considered that a slower crystal growth rate would produce cleaner and larger crystals and investigated conditions such as convection and diffusion by changing solvent viscosity, which mimics gel layer crystallization [38], to further slow down the growth rate.

We changed the viscosity of the conditions under which crystals could be crystallized by the solvent evaporation and vapor diffusion methods described above. The compound that changes the viscosity of the solution used in crystallization was examined, and ethylene glycol was considered appropriate [39].

Ethylene glycol was dissolved in a methanol solution by the solvent evaporation method, and four conditions with different viscosities were prepared for crystallization. The viscosity of the methanol solution was 0.82 mPa·s, and those with different viscosities were 0.95, 1.18, 1.10, and 1.52 mPa·s. Although we were able to increase the viscosity to about twice as high, only powder was precipitated and no crystal was formed.

In addition, the viscosity of DMF was changed by using DMF and diethyl ether, the method that produced the cleanest crystals by the vapor diffusion method (Table 7). When the viscosity was changed using ethylene glycol in the same way as above, the viscosity of DMF was 0.88 mPa·s, and those with different viscosities were 1.23, 1.76, and 2.01 mPa·s, respectively [40]. Needle-shaped crystals were obtained in all three conditions of the vapor diffusion method with varying viscosity. However, all crystals were of equal size and did not vary with viscosity.

**Table 7.** Conditions and results of the vapor diffusion method.

Good Solvent	Poor Solvent	Added Compound	Temperature/K	Viscosity/ mPa·s	Results
DMF	Diethyl ether	Ethylene glycol	297.8	0.88	Not Appeared
DMF	Diethyl ether	Ethylene glycol	294.7	1.23	Needle crystal
DMF	Diethyl ether	Ethylene glycol	297.0	1.76	Needle crystal
DMF	Diethyl ether	Ethylene glycol	296.0	2.04	Needle crystal

The specificity of chemical reactions in nanoscale space is treated as a so-called scale effect, but there remain unclear things. Namely, the factors may include dissolution and mixing at the interface, diffusion, surface tension, activation energy, solvent viscosity, and the influence of electric and magnetic fields. Examining conditions like these may seem trivial at first glance, but when reviewed from a perspective that leads to cutting-edge research, it can be seen as having challenging significance.

#### 4. Conclusions

Even in a flexible and orientation-preserving polymer film, an azo-amino acid Schiff base copper complex, which we treated for the first time, exhibited anisotropic molecular orientation induced by polarized ultraviolet light irradiation. The azo-amino acid Schiff base copper complex has a structure similar to that of related complexes that have been proven to improve the efficiency of synthesis reactions in microfluidics in the past, and the azo-amino acid Schiff base copper complex can be considered to reflect mechanical properties. When the conditions were examined as a model synthesis reaction, no clear superiority was found for the synthesis of azo-amino acid Schiff base copper complexes. It was suggested that the microscale “mechanical” environment is a unique condition. With gel crystallization in mind, we investigated the solvent type and viscosity conditions for single-crystal growth of azo-amino acid Schiff base copper complexes [41] and found that small single crystals were obtained when the combination of solvents was appropriate. It can be said that modeling the liquid–liquid equilibrium in microdroplets in a normal-scale gas-liquid equilibrium environment is partially effective.

In short, the results of testing the inverse scale effect hypothesis revealed that the inverse effect was unclear. In other words, the effect of promoting a reaction in a microscale channel or microdroplet cannot be judged solely by the dependence on element-reducing conditions such as solute diffusion and solvent viscosity on a normal scale.

**Author Contributions:** Conceptualization, T.A.; investigation, Y.W., A.K. and T.I.; writing—original draft preparation, Y.W.; writing—review and editing, T.A. and D.N.; supervision, T.A. All authors have read and agreed to the published version of the manuscript.

**Funding:** This research received no external funding.

**Institutional Review Board Statement:** Not applicable.

**Informed Consent Statement:** Not applicable.

**Data Availability Statement:** The data is unavailable due to privacy or ethical restrictions.

**Acknowledgments:** The authors thank D. Tanaka (Waseda University) for the helpful suggestion about microfluidic synthesis.

**Conflicts of Interest:** The authors declare no conflicts of interest.

#### References

1. The, S.-Y.; Lin, R.; Hung, L.-H.; Lee, A.P. Droplet microfluidics. *Lab Chip* **2008**, *8*, 198–220. [[CrossRef](#)] [[PubMed](#)]
2. Shang, L.; Cheng, Y.; Zhao, Y. Emerging Droplet Microfluidics. *Chem. Rev.* **2017**, *117*, 7964–8040. [[CrossRef](#)] [[PubMed](#)]
3. Mashaghi, S.; Abbaspurrad, A.; Weitz, D.A.; van Oijen, A.M. Droplet microfluidics: A tool for biology, chemistry, and nanotechnology. *Trends Anal. Chem.* **2016**, *82*, 118–125. [[CrossRef](#)]
4. Bawazer, T.A.; McNally, C.S.; Empson, C.J.; Marchant, W.J.; Comyn, T.P.; Niu, X.; Cho, S.; McPherson, M.J.; Binks, B.P.; deMello, A.; et al. Combinational microdroplet engineering for biomimetic material synthesis. *Sci. Adv.* **2016**, *2*, e1600567. [[CrossRef](#)] [[PubMed](#)]
5. Chung, C.H.Y.; Lau, C.M.L.; Sin, D.T.; Chung, J.T.; Zhang, Y.; Chau, Y.; Yao, S. Droplet-Based Microfluidic Synthesis of Hydrogel Microparticles via Click Chemistry-Based Cross-Linking for the Controlled Release of Proteins. *ACS Appl. Bio Mater.* **2021**, *4*, 6186–6194. [[CrossRef](#)] [[PubMed](#)]
6. Zeng, Y.; Khor, J.W.; van Neel, T.L.; Tu, W.-C.; Berthier, J.; Thongpang, S.; Berthier, E.; Theberge, A.B. Miniaturizing chemistry and biology using droplet in open systems. *Nat. Rev. Chem.* **2023**, *7*, 439–455. [[CrossRef](#)] [[PubMed](#)]
7. Song, H.; Chen, D.L.; Ismagilov, R.F. Reactions in Droplets in Microfluidic Channels. *Angew. Chem. Int. Ed.* **2006**, *45*, 7336–7356. [[CrossRef](#)] [[PubMed](#)]
8. Ibrahim, O.A.; Navarro-Segarra, M.; Dadeghi, P.; Sabate, N.; Esquivel, J.P.; Kjeang, E. Microfluidics for Electrochemical Energy Conversion. *Chem. Rev.* **2022**, *122*, 7236–7266. [[CrossRef](#)]
9. Kobayashi, M.; Akitsu, T.; Furuya, M.; Sekiguchi, T.; Shoji, S.; Tanii, T.; Tanaka, D. Efficient Synthesis of a Schiff Base Copper(II) Complex Using a Microfluidic Device. *Micromachines* **2023**, *14*, 890. [[CrossRef](#)]
10. Zafar, A.; Takeda, C.; Manzoor, A.; Tanaka, D.; Kobayashi, M.; Wadayama, Y.; Nakane, D.; Majeed, A.; Iqbal, M.A.; Akitsu, T. Towards Industrially Important Applications of Enhanced Organic Reactions by Microfluidic Systems. *Molecules* **2024**, *29*, 398. [[CrossRef](#)]

11. Moragues, T.; Arguijo, D.; Beneyton, T.; Modavi, C.; Simutis, K.; Abate, A.R.; Baret, J.-C.; deMello, A.J.; Densmore, D.; Griffiths, A.D. Droplet-based microfluidics. *Nat. Rev. Methods Primers* **2023**, *3*, 32. [[CrossRef](#)]
12. Ding, Y.; Howes, P.D.; deMello, A.J. Recent Advances in Droplet Microfluidics. *Anal. Chem.* **2020**, *92*, 132–149. [[CrossRef](#)] [[PubMed](#)]
13. Courtois, F.; Olguin, L.F.; Whyte, G.; Theberge, A.B.; Huck, W.T.S.; Hollfelder, F.; Abell, C. Controlling the Retention of Small Molecules in Emulsion Microdroplets for Use in Cell-Based Assays. *Anal. Chem.* **2009**, *81*, 3008–3016. [[CrossRef](#)] [[PubMed](#)]
14. Trinh, T.N.D.; Do, H.D.K.; Nam, N.N.; Dan, T.T.; Trinh, K.T.L.; Lee, N.Y. Droplet-Based Microfluidics: Applications in Pharmaceuticals. *Pharmaceuticals* **2023**, *16*, 937. [[CrossRef](#)] [[PubMed](#)]
15. Zhu, P.; Wang, L. Passive and active droplet generation with microfluidics: A review. *Lab Chip* **2017**, *17*, 34–75. [[CrossRef](#)]
16. Pollack, M.G.; Shenderov, A.D.; Fair, R.B. Electrowetting-based actuation of droplets for integrated microfluidics. *Lab Chip* **2002**, *2*, 96–101. [[CrossRef](#)] [[PubMed](#)]
17. Sohrabi, S.; Kassir, N.; Moraveji, M.K. Retracted Article: Droplet microfluidics: Fundamentals and its advanced applications. *RSC Adv.* **2020**, *10*, 27560–27574. [[CrossRef](#)] [[PubMed](#)]
18. Dangla, R.; Kayi, S.C.; Baroud, C.N. Droplet microfluidics driven by gradients of confinement. *Proc. Natl. Acad. Sci. USA* **2013**, *110*, 853–858. [[CrossRef](#)] [[PubMed](#)]
19. Huang, C.; Jiang, Y.; Li, Y.; Zhang, H. Droplet Detection and Sorting System in Microfluidics: A Review. *Micromachines* **2023**, *14*, 103. [[CrossRef](#)]
20. Barnes, C.; Sonwane, A.R.; Sonnenschein, E.C.; Giudice, F.D. Machine learning enhanced droplet microfluidics. *Phys. Fluids* **2023**, *35*, 092003. [[CrossRef](#)]
21. Akitsu, T. Inversely Finding Peculiar Reaction Conditions toward Microfluidic Droplet Synthesis. *Reactions* **2023**, *4*, 647–656. [[CrossRef](#)]
22. Kashiwagi, K.; Tassinari, F.; Haraguchi, T.; Banerjee-Gosh, K.; Akitsu, T.; Naaman, R. Electron Transfer via Helical Oligopeptide to Laccase Including Chiral Schiff Base Copper Mediators. *Symmetry* **2020**, *12*, 808. [[CrossRef](#)]
23. Nattansohn, A.; Rochon, P. Photoinduced Motions in Azo-Containing Polymers. *Chem. Rev.* **2002**, *102*, 4139–4175. [[CrossRef](#)] [[PubMed](#)]
24. Akitsu, T.; Yamazaki, A.; Kobayashi, K.; Haraguchi, T.; Endo, K. Computational Treatments of Hybrid Dye Materials of Azobenzene and Chiral Schiff Base Metal Complexes. *Inorganics* **2018**, *6*, 37. [[CrossRef](#)]
25. Akitsu, T.; Mitani, Y.; Nakane, D.; Aoki, K.; Lo, C.-T. Photofunctional Materials of (Bio) Polymers and Metal Complexes. In *Advances in Textile Engineering*; Open Access eBooks: Las Vegas, NV, USA, 2022; Volume 2, pp. 1–27.
26. Gruzdenko, A.; Dierking, I. Liquid crystal-based actuators. *Front. Soft Matter* **2022**, *2*, 1052037. [[CrossRef](#)]
27. Ambrosio, A.; Marrucci, L.; Borbone, F.; Roviello, A.; Maddalena, P. Light-induced spiral mass transport in azo-polymer films under vortex-beam illumination. *Nat. Commun.* **2012**, *3*, 989. [[CrossRef](#)] [[PubMed](#)]
28. Martirosyan, A.; Falke, S.; McCombs, D.; Cox, M.; Radka, C.D.; Knop, J.; Betzel, C.; DeLucas, L.J. Tracing transport of protein aggregates in microgravity versus unit gravity crystallization. *NPJ Microgravity* **2022**, *8*, 4. [[CrossRef](#)] [[PubMed](#)]
29. Makuch, K.; Holyst, R.; Kalwarczyk, T.; Garstecki, P.; Brady, J.F. Diffusion and flow in complex liquids. *Soft Matter* **2020**, *16*, 114–124. [[CrossRef](#)]
30. Filatov, N.A.; Evstrapov, A.A.; Bukatin, A.S. Negative Pressure Provides Simple and Stable Droplet Generation in a Flow-Focusing Microfluidic Device. *Micromachines* **2021**, *12*, 662. [[CrossRef](#)]
31. Yamaguchi, T. Decoupling between Solvent Viscosity and Diffusion of a Small Solute Induced by Self-Motion. *J. Phys. Chem. Lett.* **2021**, *12*, 7696–7700. [[CrossRef](#)]
32. Hartge, H.M.; Flöter, E.; Vilgis, T.A. Crystallization in highly supersaturated, agitated sucrose solutions. *Phys. Fluids* **2023**, *35*, 064120. [[CrossRef](#)]
33. Aspillaga, L.; Jan Bautista, D.; Daluz, S.N.; Hernandez, K.; Renta, J.A.; Lopez, E.C.R. Nucleation and Crystal Growth: Recent Advances and Future Trends. *Eng. Proc.* **2023**, *56*, 22. [[CrossRef](#)]
34. Velásquez-González, O.; Campos-Escamilla, C.; Flores-Ibarra, A.; Esturau-Escofet, N.; Arreguin-Espinosa, R.; Stojanoff, V.; Cuéllar-Cruz, M.; Moreno, A. Crystal Growth in Gels from the Mechanisms of Crystal Growth to Control of Polymorphism: New Trends on Theoretical and Experimental Aspects. *Crystals* **2019**, *9*, 443. [[CrossRef](#)]
35. Mady, O. Application of solvent evaporation technique for pure drug crystal spheres preparation. *Particuology* **2022**, *67*, 79–89. [[CrossRef](#)]
36. Metherall, J.P.; Carroll, R.C.; Coles, S.J.; Hall, M.J.; Probert, M.R. Advanced crystallisation methods for small organic molecules. *Chem. Soc. Rev.* **2023**, *52*, 1995–2010. [[CrossRef](#)] [[PubMed](#)]
37. McArdle, P.; Erxleben, A. Crystal growth and morphology control of needle-shaped organic crystals. *CrystEngComm* **2024**, *26*, 416–430. [[CrossRef](#)]
38. Tong, J.; de Bruyn, N.; Alieva, A.; Legge, E.J.; Boyes, M.; Song, X.; Walisinghe, A.J.; Pollard, A.J.; Anderson, M.W.; Vetter, T.; et al. Crystallization of molecular layers produced under confinement onto a surface. *Nat. Commun.* **2024**, *15*, 2015. [[CrossRef](#)] [[PubMed](#)]
39. Gavira, J.A.; Cera-Manjarres, A.; Ortiz, K.; Mendez, J.; Jimenez-Torres, J.A.; Patiño-Lopez, L.D.; Torres-Lugo, M. Use of Cross-Linked Poly(ethylene glycol)-Based Hydrogels for Protein Crystallization. *Cryst. Growth Des.* **2024**, *14*, 3239–3248. [[CrossRef](#)]

40. Bernal-García, J.M.; Guzmán-López, A.; Cabrales-Torres, A.; Estrada-Baltazar, A.; Iglesias-Silva, G.A. Densities and Viscosities of (N,N-Dimethylformamide + Water) at Atmospheric Pressure from (283.15 to 353.15) K. *J. Chem. Eng. Data* **2008**, *53*, 1024–1027. [[CrossRef](#)]
41. Kaneda, A.; Suzuki, S.; Nakane, D.; Kashiwagi, Y.; Akitsu, T. Crystal structure and Hirshfeld surface analysis of (1*H*-imidazole- $\kappa N^3$ )[4-methyl-2-([2-oxido-5-(2-phenyldiazen-1-yl)phenyl]methylidene)amino]pentanoate- $\kappa^3 O, N, O'$ ]copper(II). *Acta Cryst. E* **2024**, *80*, 468–471. [[CrossRef](#)]

**Disclaimer/Publisher's Note:** The statements, opinions and data contained in all publications are solely those of the individual author(s) and contributor(s) and not of MDPI and/or the editor(s). MDPI and/or the editor(s) disclaim responsibility for any injury to people or property resulting from any ideas, methods, instructions or products referred to in the content.